Analysis of the Forming of Interlock Textile Composites Using a Hypoelastic Approach

Bo Chen, Philippe Boissé, Julien Colmars, Naïm Naouar, Renzi Bai, Philippe Chaudet

Applied Composite Materials (2021), 1-16
https://doi.org/10.1007/s10443-021-09966-z

Analysis of the Forming of Interlock Textile Composites Using a Hypoelastic Approach

B. Chen [1] · **P. Boisse** [1] · **J. Colmars** [1] · **N. Naouar** [1] · **R. Bai** [1] · **P. Chaudet** [1]

[1] Université de Lyon, LaMCoS, CNRS, INSA-Lyon, 69621 Villeurbanne, France

Abstract

Numerical simulation of the textile composites forming plays an important role in improving the manufacturing quality, reducing the manufacturing cycle, and manufacturing cost. The focus is on the shaping of one or several layers of G1151 interlock reinforcement. Based on the continuous approach at the macroscale, an approach using a hypoelastic behavior is proposed considering the specific interlock textile material behavior. The stress accumulation is carried out in frames defined by the direction of the warp and weft yarns. The approach is implemented in the commercial software Abaqus. By adding inter-layer contact properties, this approach can realize the simulation of multi-layers textile composites with different yarn orientation configurations. Experimental analyses have shown that this approach can correctly trace the specific behavior of interlock textile composites.

Keywords Interlock fabric · Hypoelastic · Forming simulation · Multi-layer

1 Introduction

Due to their excellent performance, the interlock textile composites are becoming more and more widely used in different areas [1–3]. These materials offer a number of attrac- tive properties: the high capacity to conform to complicated contours, suitable for manufacturing components with complex shapes, and greater flexibility in processing options compared to metals. Numerical analysis of the textile composite materials has become a hot topic in the past several decades [4–6].

The tows (also called yarns) of interlock fabric are made of continuous fibers with a very small diameter ranging from 5 to 15 μm. These yarns are held together by weaving into the interlock fabric, which makes it possible to consider this material as a continuum medium at the macroscopic scale for numerical analysis. In the presented research, a numerical continuous approach will be developed at the macroscale, the interlock fabric is not continuous at lower scales (microscales and mesoscales) but it can be considered as continuous on average at macroscopic scale [5, 7]. Performing numerical analysis at macroscale will decrease the number of finite elements to model

✉ B. Chen
bo.chen@insa-lyon.fr

the material geometry, and wrinkles is one of the main defects which occurs at macroscopic scale [8–10]. The advantage of applying the continuous approach in numerical simulation lies in using finite elements to develop the numerical model of the textile reinforcement.

For single layer interlock textile composites, the dimension in the thickness direction is much smaller than the other two directions, thus, shell elements can be adapted to model single layer textile composites. The slippage between fibers gives very specific mechanical properties, in order to correctly trace the material properties at the macroscale, some research works were devoted to the shell formulation development. Soulat et al. [11] developed a shell element considering the stress through the thickness, Liang et al. and Renzi et al. [12, 13] developed specific shell approaches based on the physics of the deformation of fibrous materials.

The objective of the presented work is dedicated to developing a hypoelastic approach within the framework of continuum mechanics to correctly predict the textile reinforcement deformation. In this article, the textile reinforcement considered is an interlock G1151 manufactured by Hexcel. The introduction of the hypoelastic model will be presented in Sect. 2. Three types of material properties which are tensile stiffness, in-plane shear stiffness, and out-of-plane bending stiffness will be considered (Fig. 1). Their influences on the forming and wrinkles formation have been well analyzed in [10]. The way to determine these material rigidities for the presented approach will be introduced in Sect. 3, and also the presented approach will be validated in terms of in-plane shear behavior and bending behavior. Section 4 is the forming of a reinforcement made of two layers of interlock fabric with different orientations. The punch shape is tetrahedron, and the corresponding simulation based on the proposed hypoelastic approach is compared with experiment results. It is indicated that the approach can correctly trace the specific behavior of interlock textile composites.

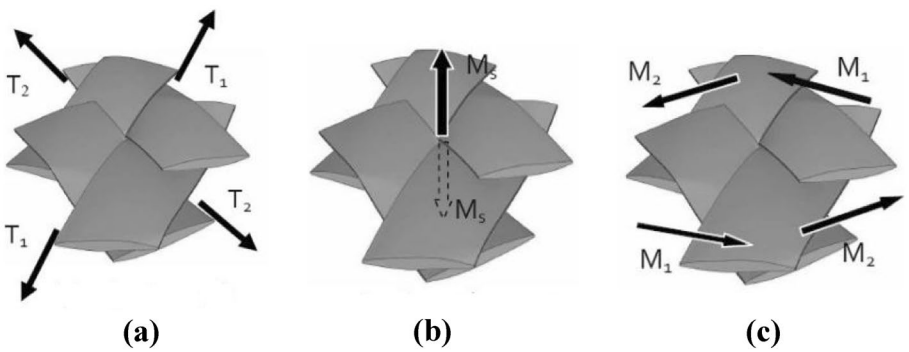

Fig. 1 Three material behavior to be considered. (**a**) Tensile. (**b**) In-plane shear. (**c**) Out-of-plane bending

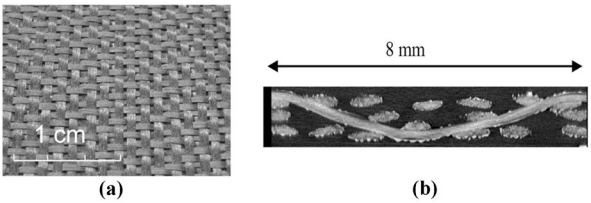

Fig. 2 (**a**) G1151 fabric structure. (**b**) X-ray Tomography of G1511 fabric (cut along warp yarn) [14]

2 The Continuous Approach with a Hypoelastic Law

2.1 The Studied Interlock Fabric

The interlock reinforcement G1151® analyzed in the present work is shown in Fig. 2a. Figure 2b shows its architecture obtained by X-ray tomography. Table 1 shows the geometric and physical characteristics of the woven reinforcement.

2.2 Frames of the Yarns

For interlock fabric material, the material properties highly depend on the yarn directions. These two yarn directions (called warp and weft) are perpendicular in the initial configuration, and they will not keep orthogonal due to the in-plane shear strain when the material deformed. Thus in order to correctly calculate the shell stress using the material constitutive equations according to the strain, it is necessary to write the constitutive equation in frames defined by the yarns [15, 16].

Hypoelastic law is widely used at large strains in the finite element analyses [17–20] and is defined as:

$$\sigma^{\nabla} = \mathbf{C} : \mathbf{D} \tag{1}$$

Here $\mathbf{D}$ is the Eulerian tensor of strain rate, $\mathbf{C}$ is the Eulerian material constitutive tensor, σ^{∇} is an objective derivative of σ which is the Eulerian tensor of Cauchy stress. There are two commonly used approaches to calculate the objective derivative stress: Jaumann corotational formulation (based on the corotational frame rotation) [21] and Green-Naghdi (GN) approach

Table 1 Geometric characteristics of the G1151 interlock fabric

Material	G1151 fabric
Manufacturer	Hexcel
Fibers	Carbon 6 K
Areal density	630 g/m^2
Single layer thickness	1.3 mm
Yarn width	Warp: 1.92 mm Weft: 2.21 mm
Yarn density	Warp: 7.5 yarns/cm Weft: 7.4 yarns/cm

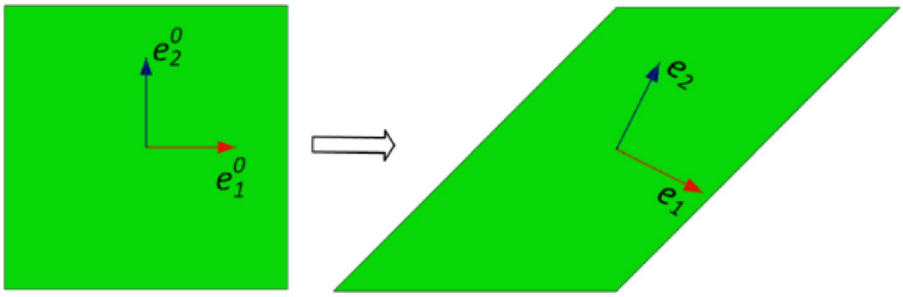

Fig. 3 Rotation of Green-Naghdi frame in a simple shear simulation test

(based on the polar rotation) [22] which is adopted in Abaqus/Explicit. Figure 3 shows a simple shear simulation test conducted in Abaqus/explicit, e (e1, e2) is the GN framework, it can be seen that the frame rotates with the deformation, however, its axis won't keep in the direction of the yarn which is necessary in the case for textile composites. Thus the GN framework cannot be used for the interlock fabric directly.

Two independent orthogonal yarn frames are constructed where each one is based on one of yarn directions, as shown in the Fig. 4, they are the frame $f_1(\mathbf{f}_1, \frac{\mathbf{f}^2}{\|\mathbf{f}^2\|})$ and the frame $f_2(\frac{\mathbf{f}^1}{\|\mathbf{f}^1\|}, \mathbf{f}_2)$. Here $\mathbf{f}_\alpha \cdot \mathbf{f}^\beta = \delta_\alpha^\beta$(the index α and β represent the warp and weft yarns, ranging from 1 to 2. δ_α^β is the Kronecker symbol, and equal to 1 when $\alpha = \beta$ and 0 otherwise. The covariant vectors $\mathbf{f}_1$ and $\mathbf{f}_2$ represent the two textiles yarn direction, the contravariant vectors $\mathbf{f}^1$ and $\mathbf{f}^2$ are perpendicular to the other yarn direction.

GN frame rotates along the polar rotation, $\mathbf{R}$ obtained from the decomposition of the deformation gradient $\mathbf{F}$.

$$\mathbf{R} = \mathbf{F}\mathbf{U}^{-1} \tag{2}$$

Then the GN frame axes $\mathbf{e}_\alpha$ at the deformed configuration can be determined using:

$$\mathbf{e}_\alpha = \mathbf{R} \cdot \mathbf{e}_\alpha^0 \tag{3}$$

For the two yarn frames, $\mathbf{f}_1$ and $\mathbf{f}_2$ will rotate along with the yarn rotation, they can be calculated using the deformation gradient tensor $\mathbf{F}$ and the textiles yarn direction in the initial configuration $\mathbf{f}_\alpha^0$:

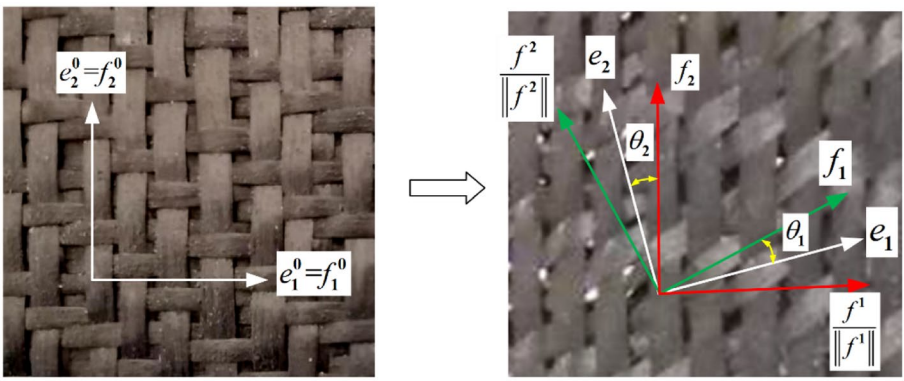

Fig. 4 The Green-Naghdi frame and the fiber frame

$$\mathbf{f}_\alpha = \frac{\mathbf{F}\cdot\mathbf{f}_\alpha^0}{\left\|\mathbf{F}\cdot\mathbf{f}_\alpha^0\right\|} = \frac{\mathbf{F}\cdot\mathbf{e}_\alpha^0}{\left\|\mathbf{F}\cdot\mathbf{e}_\alpha^0\right\|} \tag{4}$$

Here $\mathbf{f}_\alpha^0$ and $\mathbf{e}_\alpha^0$ are unit vectors and are assumed to be coincide initially. Let θ_α be the angle between GN axes and the two yarn axes, the transform matrix $\left[T_\alpha\right]$ between GN frame and the two yarn frames f_1, f_2 will be:

$$\left[T_\alpha\right] = \begin{bmatrix} \cos\theta_\alpha & -\sin\theta_\alpha \\ \sin\theta_\alpha & \cos\theta_\alpha \end{bmatrix} \tag{5}$$

2.3 Hypoelastic Law for Interlock Fabric

The hypoelastic law used in textiles fabric forming has been researched in several studies [15, 16, 23, 24]. In hypoelastic law, the material behavior is described using a relationship between an objective stress derivative and the strain rate. The material behavior can be linear or non-linear.

In the case of the interlock fabric, the objective stress derivative is based on the two built fiber frames shown in Fig. 4, the objective derivative of the Cauchy stress tensor with respect to fiber rotation tensor is:

$$\sigma^\nabla = \Delta\cdot\left(\frac{d}{dt}\left(\Delta^T\cdot\sigma\cdot\Delta\right)\right)\cdot\Delta^T \tag{6}$$

Here Δ is the rotation matrix from the initial frame to the yarn frame. In order to apply the hypoelastic law for fabric material, at each numerical analysis time step, the strain increments in the GN frame will be firstly transformed to the two yarn frames to obtain the yarn strain increments using the transform matrix $\left[T_\alpha\right]$ (Eq. (5))

$$[d\varepsilon]_{f_\alpha} = \left[T_\alpha\right][d\varepsilon]_e\left[T_\alpha\right] \tag{7}$$

The strain increments are used to calculate the components of section stress increments in the two yarn frames:

$$[d\sigma]_{f_\alpha} = [C]_{f_\alpha}[d\varepsilon]_{f_\alpha} \tag{8}$$

Here $[C]_{f_\alpha}$ is the material stiffness, it will be determined in the Sect. 3. Following the incremental formulation of Hughes and Winget [Hughes 1980], total section stress at the time step t_{n+1} in the two yarn frames can be obtained using mid-point integration as followed:

$$\left[\sigma^{n+1}\right]_{f_\alpha^{n+1}} = \left[\sigma^n\right]_{f_\alpha^n} + [d\sigma]_{f_\alpha^{n+1/2}} \tag{9}$$

The total section stress $[\sigma]_{f_\alpha}$ in the two yarn frames will be expressed in the GN frame to get the section stress $[\sigma]_e$(n + 1 index is omitted, all the quantities are at t_{n+1})

$$[\sigma]_e = \left[T_1\right][\sigma]_{f_1}\left[T_1\right]^T + \left[T_2\right][\sigma]_{f_2}\left[T_2\right]^T \tag{10}$$

2.4 Decoupling Bending Behavior with Membrane

Due to the possible relative slippage between warp and weft yarns, the interlock fabric bending stiffness is much lower than the bending stiffness provided by a classical theory for a given membrane stiffness. This lower bending stiffness has caused the bending behavior to be neglected in some previous researches on the textiles forming simulation [15, 25–29]. However, some studies have shown that the bending stiffness plays a significant role on the textile material forming, especially on wrinkles forming and development [10, 30, 31]. Figure 5 shows the wrinkling of textile material with different bending stiffness when compressed in the yarn direction.

For single layer textile composites, the dimension in the thickness direction is much smaller than the other two directions, thus, shell element is adopted to model single layer textile composites. In the shell element, the bending stiffness is general coupled with membrane behavior, for the classical continuous material, it can be directly obtained as followed:

$$B_{classic} = \frac{Eh^3}{12\left(1-\nu^2\right)} \tag{11}$$

Here E is the Young's modulus, h is the shell thickness, and ν is the Poison's ratio. This is not the case for the interlock fabric. In order to properly consider the bending behavior in the interlock fabric forming simulation, Dobrich et al. [32] proposed a laminated shell approach, this approach can decouple the bending and membrane stiffness by changing the properties in the different layers of the laminate points in the thickness direction. Other approaches focus on the superimposition of different elements, these elements share the same nodes, and the membrane and bending behavior will be implemented with different Young's modulus [16, 33, 34].

These approaches may be effective in some cases, but they are not based on the material deformation mechanism, and will lead to an increment in the element number. An independent moment–curvature relation will be introduced, and this relationship is tested by bending experiment test in Sect. 3.2. The membrane and bending response will be calculated separately in the presented approach which is implemented in the Abaqus software.

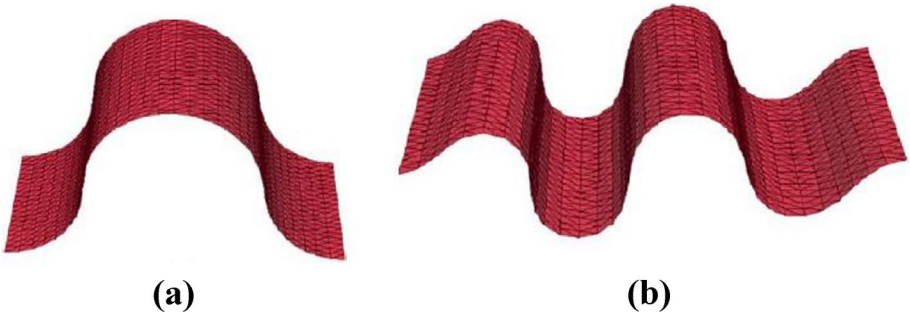

Fig. 5 Compression in the yarn direction of a textile material with different bending stiffness [10]. (**a**) $B = 1$ Nmm. (**b**) $B = 10$ Nmm

3 Characterization of In-Plane Shear and Bending Behaviors

In this section, the membrane and bending properties of the G1151 interlock fabric will be determined and the presented modeling approach will be validated. As for the material tensile stiffness, its large value leads to the quasi-inextensibility in the yarn direction. It is assumed to be constant.

3.1 Bias Extension Test

This chapter is to determine the material in-plane shear behavior, and on this basis, verify the in-plane shear response of the presented approach in the woven reinforcement simulation. The bias extension test is conducted. As shown in Fig. 6a, a rectangular specimen is under the tensile deformation, where the warp and weft yarns are at $\pm$ 45° in the ten- sile direction. Neglecting the slippage between warp and weft yarn and assuming being

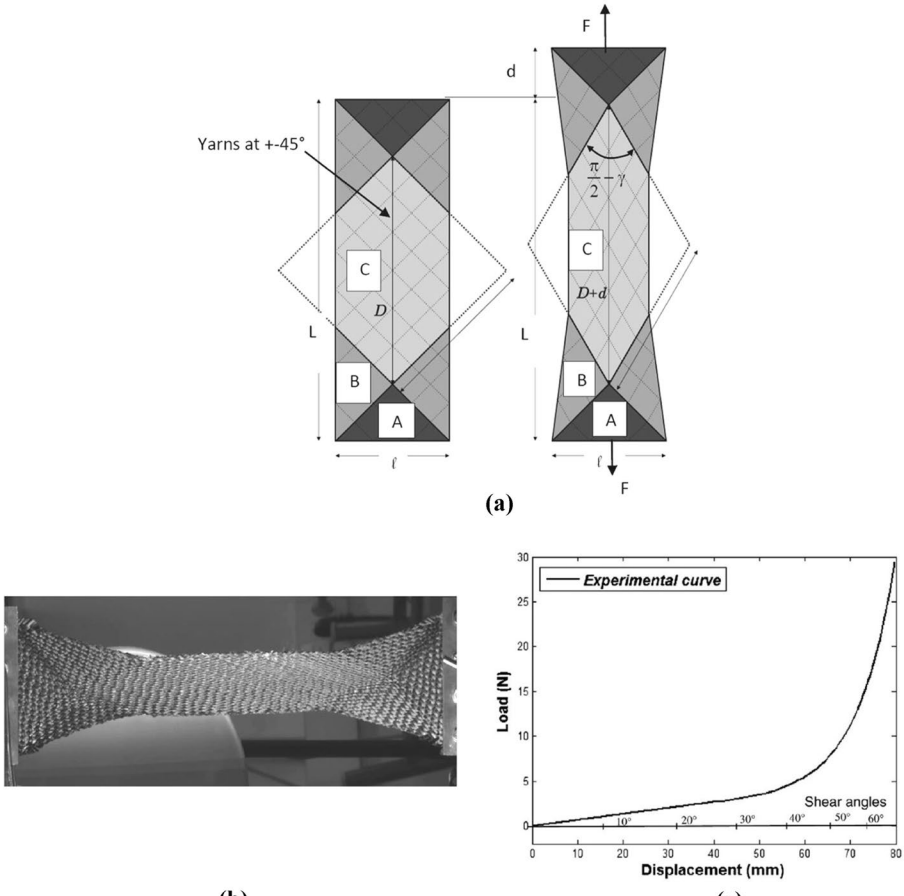

Fig. 6 Bias extension test. (**a**) Schematic diagram. (**b**) Experiment deformed specimen. (**c**) load–displacement curve of G1151 interlock fabric

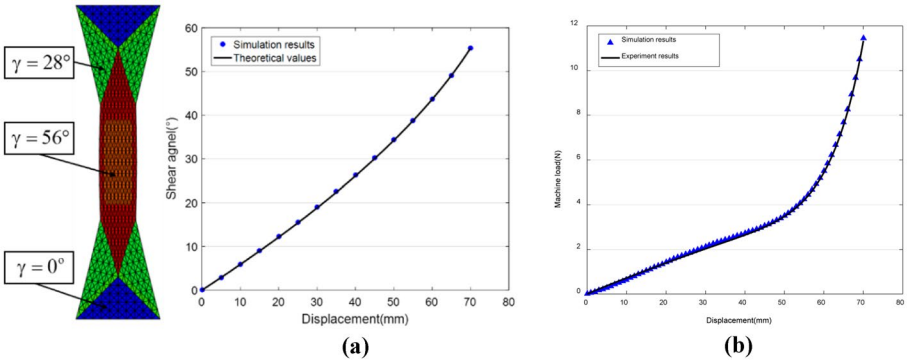

Fig. 7 Bias extension test verification in different displacement. (**a**) Shear angle comparison. (**b**) Machine load comparison

inextensible in the yarn direction, there will be three different shear zones when the specimen is deformed, and the shear angle will be constant in each shear zone. The center zone C has two free ends, the shear angle in zones B is half of zone C, and the shear angle in zone A is zero.

The theoretical values of shear angle at the zone C is related to the tensile displacement:

$$\gamma = \frac{\pi}{2} - 2\arccos\left(\frac{D+d}{\sqrt{2}D}\right) \tag{12}$$

Figure 6b shows the bias extension experiment test, and the G1151 interlock fabric experiment result of load–displacement curve is given in Fig. 6c. The initial length of the specimen in the experiment is 300 mm which is three times of the width of the specimen.

According to the energy conservation, the machine load–displacement can be converted into the curve of shear force- shear angle [35, 36]. Through the polynomial fitting, the function between shear force and shear angle (radians) can be obtained, and finally, the in-plane shear stiffness G_{12} can be obtained by deriving the function. The in-plane shear stiffness G_{12} of the G1151 interlock fabric is obtained as a function of the shear angle γ:

$$G_{12} = 0.088 - 0.828\gamma + 2.924\gamma^2 - 4.008\gamma^3 + 2.031\gamma^4 \tag{13}$$

The numerical test is conducted using the in-plane shear stiffness G_{12} given in Eq. (13). The 3-node shell element has been selected for the numerical analysis. The shear angle comparison between simulation results and theoretical values calculated by Eq. (12) is shown in Fig. 7a, and the load force comparison between experiment and simulation is plotted in Fig. 7b. Good agreements have been obtained which indicated that the introduced approach can correctly describe the interlock fabric in-plane shear response.

3.2 Cantilever Bending Test

In order to test the G1151 interlock fabric bending behavior and verify the presented approach and bending response, the cantilever experiment and corresponding simulation test are conducted. In the cantilever test, the specimen shape is rectangular and two yarn directions are parallel to two sides of the rectangular respectively, one end of the specimen is

clamped, and the other is bent under the gravity [37, 38]. Figure 8a and c show the two G1151 fabric cantilever tests bending along warp and weft yarn direction respectively. The cantilever bending section length is 180 mm, and the width is 50 mm. The two rulers in the pictures build an orthogonal coordinate system for the experiments.

Through image processing, the section curve can be obtained by polynomial fitting, set the section curve formula as $y = f(x)$, then the curvature $\kappa(x)$ at different location can be expressed as:

$$k(x) = \frac{f'(x)}{\left[1 + \left[f'(x)\right]^2\right]^{3/2}} \tag{14}$$

The bending moment can be determined by the location and the material density:

$$M(s) = \int_s^L q(u - s)\cos\left(\phi(u)\right)du \tag{15}$$

Here s is the curvilinear coordinate of the point, q is the weight per unit length of the specimen(N/mm), L is the total bending section length, μ and ϕ are the Frenet's coordinates of the point.

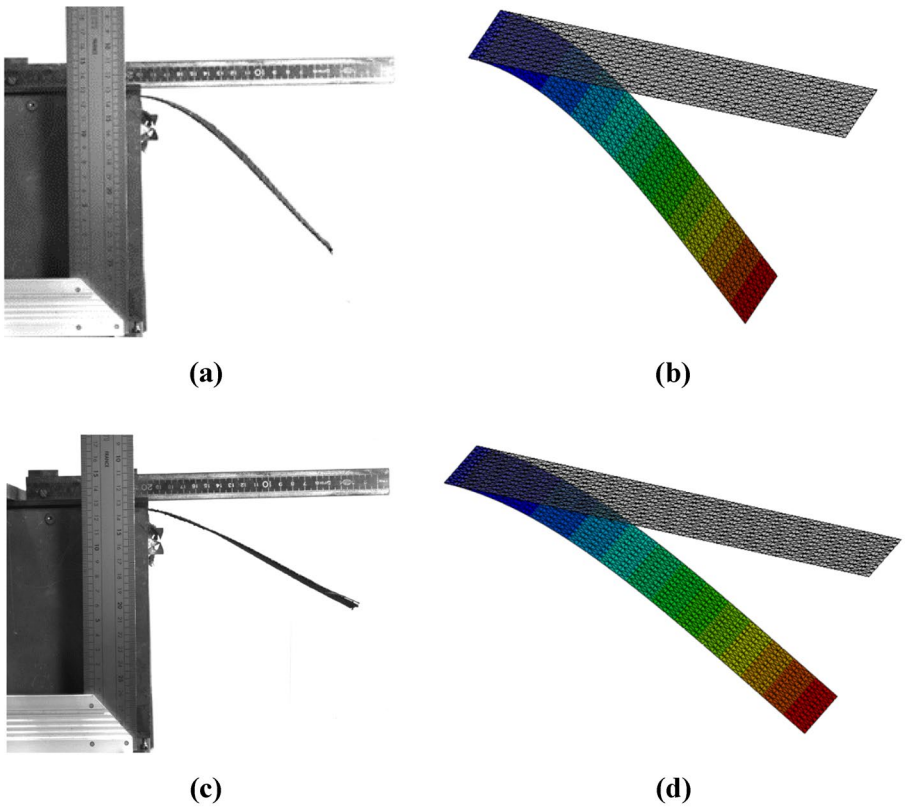

Fig. 8 Cantilever test of G1151 interlock fabric. (**a**) Bending experiment alone warp yarn (**b**) Bending simulation alone warp yarn (**c**) Bending experiment alone weft yarn (**d**) Bending simulation alone weft yarn

The moment–curvature relation $M(\kappa)$ can be obtained through combining Eqs. (14) and (15), then the bending stiffness will be determined by deriving the moment–curvature relation. Through processing the cantilever experiment in Fig. 8a and c, the material bending stiffness can be approximately regarded as linear, and the bending stiffness along warp and weft yarn direction of G1151 interlock fabric are:

$$B_1 = 10.5\,Nmm\,B_2 = 4.3\,Nmm \tag{16}$$

Applying the tested material bending stiffness, the corresponding cantilever simulation test is conducted using the presented approach. The mesh setting is the same as bias extension test in Sect. 3.1. The simulation results in the warp and weft yarn directions are shown in Fig. 8b and d respectively. Then the bending deformed section shapes of experiment and simulation are chosen as the comparison values, the comparison results are shown in Fig. 9, and can be seen there is a good agreement between the simulation and experiment. Through the comparison, it can be known that the presented approach well achieved the decoupling of bending behavior and membrane and can correctly describe the fabric bending response.

For simplicity, the difference between warp and weft yarn direction can be neglected and an average bending stiffnesses is adopted in the subsequent forming simulation.

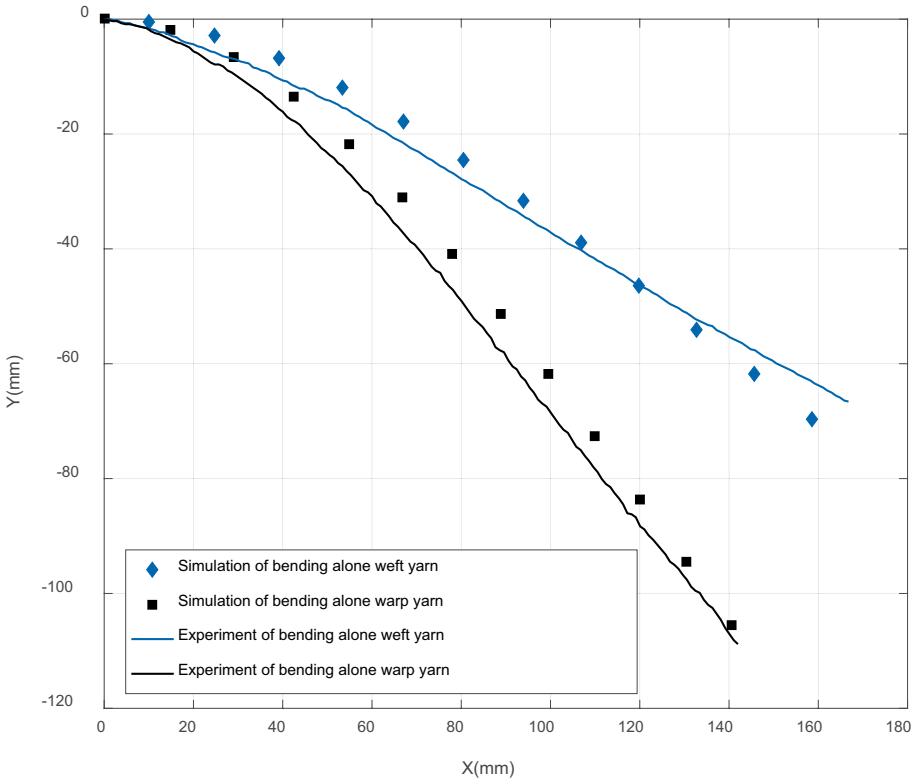

Fig. 9 Simulation and experiment results of bending section shape

4 Interlock Fabric Forming Experiment and Simulation

To examine the capabilities of the presented hypoelastic approach, the experimental test and the corresponding simulation are compared to check if the approach is able to correctly predict the material deformation in the forming process.

4.1 Tetrahedron Forming Experiment

The geometry parameter of the tetrahedron forming is described in the Fig. 10, two-layer with $[90°/0°, -45°/45°]$ (quasi-isotropic) lay-up is used in the forming experiment, and the initial dimension of each layer is 300 mm × 300 mm. The thickness of blank holder and the die mold are 30 mm and all are transparent in order to observe the material deformation in the forming process, and two cameras are used to capture pictures from the top side view and the bottom side view respectively. The forming speed of punch is set to 30 mm/min and the punch final displacement is 90 mm. The blank holder and die mold are fixed to make sure the distance between them remains constant in the forming process. This forming process is under the room temperature.

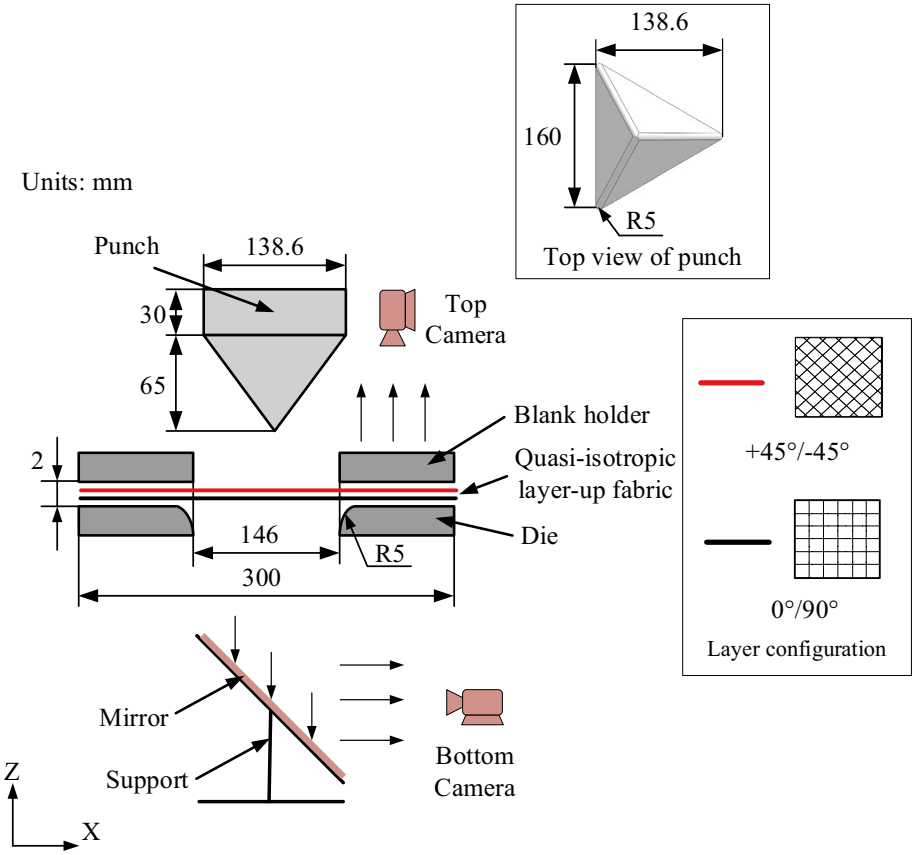

Fig. 10 Geometry parameter of the tetrahedron shape

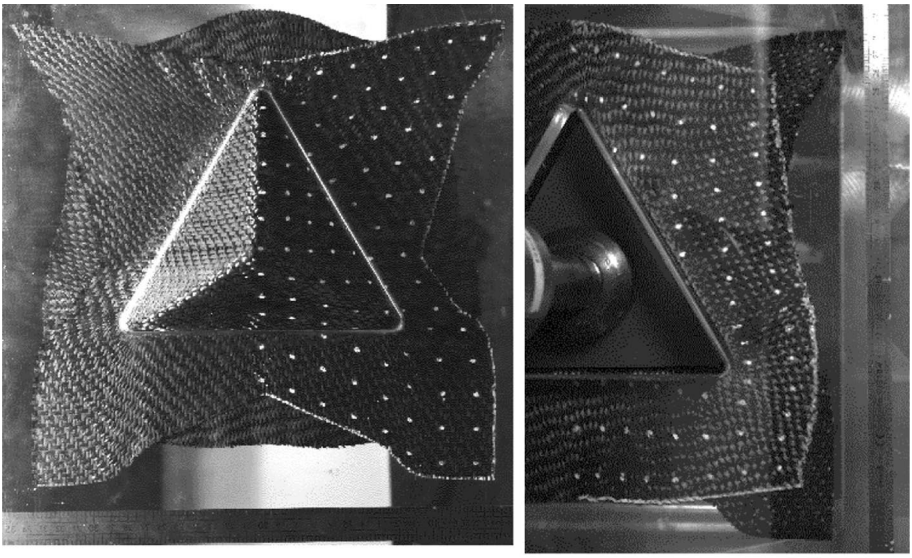

Fig. 11 Experimental pictures of two-layer quasi-isotropic c tetrahedron forming. (**a**) Bottom view. (**b**) Top view

When preparing the material, white dots are painted on the material at equal intervals to track the material movement at different position. The distance between adjacent white dots is 20 mm. The distance between the white dots and the material edge is 10 mm. The material edge is also painted in white to get the edge deformation. The final forming shape is as shown in Fig. 11, the deformation of $0°/90°$ layer is shown in the bottom view result (Fig. 11a), and the top view result shows the deformation the layer of $+45°/-45°$ (Fig. 11b).

4.2 Tetrahedron Forming Simulation

The presented approach is implemented in the commercial software Abaqus. In the modelling process, the punch, die mold and blank-holder are set as rigid body because the deformation is small compared with the fabric deformation. The forming simulation performed over half of the fabric, and 20,000 triangular shell elements are used for each layer. For the contact properties, Coulomb friction coefficients of adjacent layers and ply-to-tool were assumed as constant 0.2 in the forming process. The mechanical properties of the interlock fabric used in the experimental tests, and required as input for the simulation were presented in Sect. 3. In the simulation, the speed of the rigid punch surface is set to 2 mm/s. The blank-holder and die mold is set as fixed, and the distance between them is keep as constant which is same as the experiment setting.

The final two-layer lay-up deformed simulation shape and the comparison with experiment are shown in Fig. 12, no wrinkles are observed in both experiment and simulation, and the simulation has good agreement with the experiment.

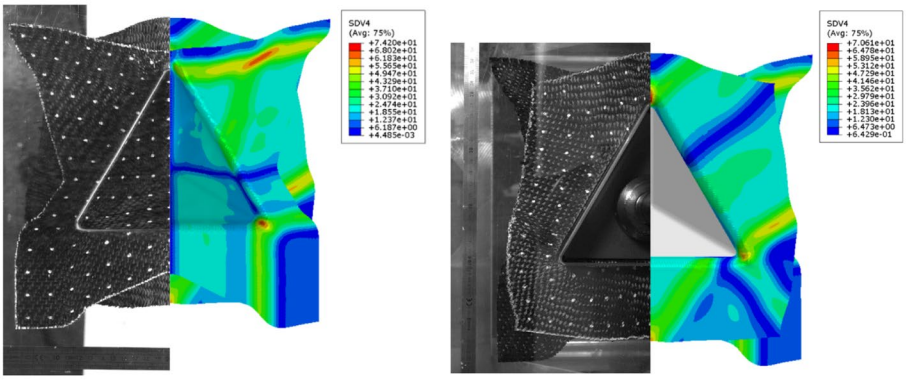

Fig. 12 Final shape comparison of experiment and simulation result (SDV4: In-plane shear angle) (**a**) Bottom 0°/90° layer (**b**) Top ±45° layer

The material drawn-in is selected as a comparison value between experiment and simulation, eleven points are selected as the comparison marker points shown in Fig. 13. The points from A to K are the location in the initial fabric, and A' to K' represent the position in the deformed fabric. The material draw-in comparison results between simulation and experiment are shown in Fig. 14, it is shown that the simulation results have good agreement with experiments at different fabric orientation.

Fig. 13 Material draw-in points position for tetrahedral forming

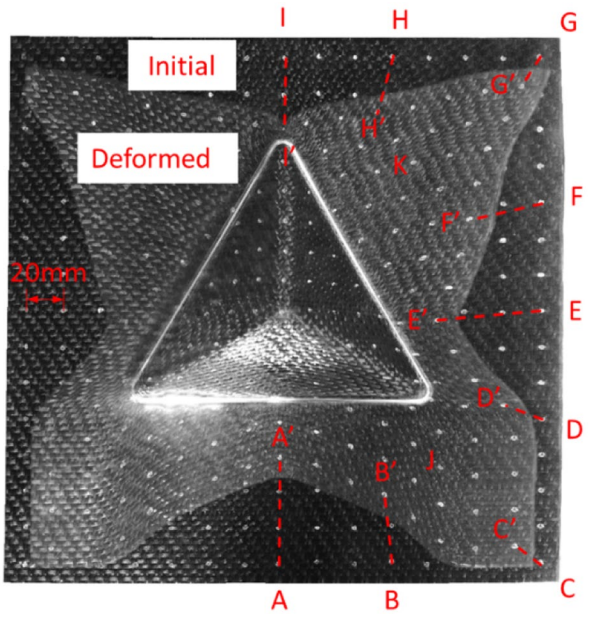

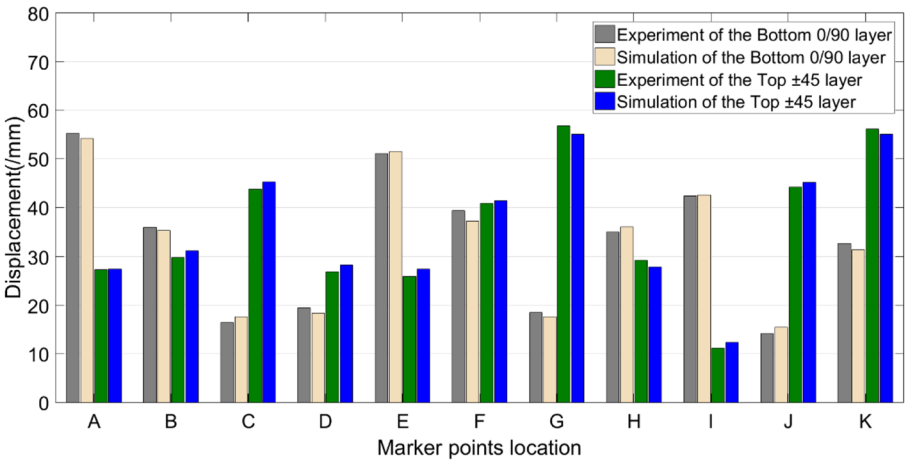

Fig. 14 Tetrahedral forming material draw-in comparison between simulation and experiment

5 Conclusion

A hypoelastic approach considering the specificity of material behavior is presented for the interlock fabric forming simulation. Due to the material behavior highly dependent on the yarn direction, it is necessary to track the two fiber yarns direction in order to calculate the stress response. The stress response is calculated separately in terms of membrane and bending in a shell element respectively, which achieves the decoupling the bending behavior with the membrane behavior. Specific to the G1151 interlock fabric, the hypoelastic law is determined through a set of experiments. Through the comparison between a tetrahedron shape forming experiment and simulation, it is found that the presented approach is accurate and robust. The approach is implemented in the commercial software Abaqus, which makes it possible for users to easily conduct the interlock fabric material forming simulation.

Acknowledgements This work was supported by the ANR, (French Research Agency), grant N° ANR-16-CE08-0042-02 COMP3DRE and by the China Scholarship Council (CSC) (B. Chen).

Data Availability The datasets generated during and/or analyzed during the current study are available from the corresponding author on reasonable request.

References

1. Chen, X., Lo, W.-Y., Tayyar, A.E., Day, R.J.: Mouldability of Angle-Interlock Woven Fabrics for Technical Applications. Text. Res. J. **72**, 195–200 (2002). https://doi.org/10.1177/004051750207200302
2. Boussu, F.: The use of warp interlock fabric inside textile composite protection against ballistic impact. Text. Res. J. **81**, 344–354 (2010). https://doi.org/10.1177/0040517510385170
3. Karaduman, NS.: Textile Reinforced Structural Composites for Advanced Applications. In: Karaduman Y, editor., Rijeka: IntechOpen; 2017, p. Ch. 4. https://doi.org/10.5772/intechopen.68245
4. Boisse, P.: Finite element analysis of composite forming. Compos. Form. Technol. A Vol. Woodhead Publ. Ser. Text., Elsevier Ltd; 2007, p. 46–79. https://doi.org/10.1533/9781845692537.46
5. Gereke, T., Döbrich, O., Hübner, M., Cherif, C.: Experimental and computational composite textile reinforcement forming: A review. Compos. Part A Appl. Sci. Manuf. **46**, 1–10 (2013). https://doi.org/10.1016/j.compositesa.2012.10.004

6. Bussetta, P., Correia, N.: Numerical forming of continuous fibre reinforced composite material: A review. Compos. Part A Appl. Sci. Manuf. **113**, 12–31 (2018). https://doi.org/10.1016/j.compositesa.2018.07.010
7. Boisse, P., Hamila, N., Madeo, A.: The difficulties in modeling the mechanical behavior of textile composite reinforcements with standard continuum mechanics of Cauchy. Some possible remedies. Int. J. Solids Struct. **154**, 55–65 (2018). https://doi.org/10.1016/j.ijsolstr.2016.12.019
8. Skordos, A.A., Monroy Aceves, C., Sutcliffe, M.P.F.: A simplified rate dependent model of forming and wrinkling of pre-impregnated woven composites. Compos. Part A Appl. Sci. Manuf. **38**, 1318–1330 (2007). https://doi.org/10.1016/j.compositesa.2006.11.005
9. Potter, K., Khan, B., Wisnom, M., Bell, T., Stevens, J.: Variability, fibre waviness and misalignment in the determination of the properties of composite materials and structures. Compos. Part A Appl. Sci. Manuf. **39**, 1343–1354 (2008). https://doi.org/10.1016/j.compositesa.2008.04.016
10. Boisse, P., Hamila, N., Vidal-Sallé, E., Dumont, F.: Simulation of wrinkling during textile composite reinforcement forming. Influence of tensile, in-plane shear and bending stiffnesses. Compos. Sci. Technol. **71**, 683–692 (2011). https://doi.org/10.1016/j.compscitech.2011.01.011
11. Soulat, D., Cheruet, A., Boisse, P.: Simulation of continuous fibre reinforced thermoplastic forming using a shell finite element with transverse stress. Comput. Struct. **84**, 888–903 (2006). https://doi.org/10.1016/j.compstruc.2006.02.011
12. Liang, B., Colmars, J., Boisse, P.: A shell formulation for fibrous reinforcement forming simulations. Compos. Part A Appl. Sci. Manuf. **100**, 81–96 (2017). https://doi.org/10.1016/j.compositesa.2017.04.024
13. Bai, R., Colmars, J., Naouar, N., Boisse, P.: A specific 3D shell approach for textile composite reinforcements under large deformation. Compos. Part A Appl. Sci. Manuf. **139**, 106135 (2020). https://doi.org/10.1016/j.compositesa.2020.106135
14. Badel, P., Vidal-Sallé, E., Maire, E., Boisse, P.: Simulation and tomography analysis of textile composite reinforcement deformation at the mesoscopic scale. Compos. Sci. Technol. **68**, 2433–2440 (2008). https://doi.org/10.1016/j.compscitech.2008.04.038
15. Khan, M.A., Mabrouki, T., Vidal-Sallé, E., Boisse, P.: Numerical and experimental analyses of woven composite reinforcement forming using a hypoelastic behavior. Application to the double dome benchmark. J. Mater. Process. Technol. **210**, 378–388 (2010). https://doi.org/10.1016/j.jmatprotec.2009.09.027
16. Thompson, A.J., Belnoue, J.P.H., Hallett, S.R.: Modelling defect formation in textiles during the double diaphragm forming process. Compos. Part B Eng. **202**, 108357 (2020). https://doi.org/10.1016/j.compositesb.2020.108357
17. Hughes, T.J.R., Winget, J.: Finite rotation effects in numerical integration of rate constitutive equations arising in large-deformation analysis. Int. J. Numer. Methods Eng. **15**, 1862–1867 (1980). https://doi.org/10.1002/nme.1620151210
18. Xiao, H., Bruhns, O.T., Meyers, A.: Hypo-Elasticity Model Based upon the Logarithmic Stress Rate. J. Elast. **47**, 51–68 (1997). https://doi.org/10.1023/A:1007356925912
19. Belytschko, T., Liu, WK., Moran, B.: Nonlinear Finite Elements for Continua and Structures 2000
20. Boisse, P., Aimène, Y., Dogui, A., Dridi, S., Gatouillat, S., Hamila, N., et al.: Hypoelastic, hyperelastic, discrete and semi-discrete approaches for textile composite reinforcement forming. Int. J. Mater. Form. **3**, 1229–1240 (2010). https://doi.org/10.1007/s12289-009-0664-9
21. Dafalias, Y.F.: Corotational Rates for Kinematic Hardening at Large Plastic Deformations. J. Appl. Mech. **50**, 561–565 (1983). https://doi.org/10.1115/1.3167091
22. Dienes, J.K.: On the analysis of rotation and stress rate in deforming bodies. Acta. Mech. **32**, 217–232 (1979). https://doi.org/10.1007/BF01379008
23. Peng, X.Q., Cao, J.: A continuum mechanics-based non-orthogonal constitutive model for woven composite fabrics. Compos. Part A Appl. Sci. Manuf. **36**, 859–874 (2005). https://doi.org/10.1016/j.compositesa.2004.08.008
24. Pierce, R.S., Falzon, B.G., Thompson, M.C.: A multi-physics process model for simulating the manufacture of resin-infused composite aerostructures. Compos. Sci. Technol. **149**, 269–279 (2017). https://doi.org/10.1016/j.compscitech.2017.07.003
25. Boisse, P., Cherouat, A., Gelin, J.C., Sabhi, H.: Experimental study and finite element simulation of a glass fiber fabric shaping process. Polym. Compos. **16**, 83–95 (1995). https://doi.org/10.1002/pc.750160111
26. Yu, W.R., Zampaloni, M., Pourboghrat, F., Chung, K., Kang, T.J.: Analysis of flexible bending behavior of woven preform using non-orthogonal constitutive equation. Compos. Part A Appl. Sci. Manuf. **36**, 839–850 (2005). https://doi.org/10.1016/j.compositesa.2004.10.026

27. ten Thije, R.H.W., Akkerman, R., Huétink, J.: Large deformation simulation of anisotropic material using an updated Lagrangian finite element method. Comput. Methods Appl. Mech. Eng. **196**, 3141–3150 (2007). https://doi.org/10.1016/j.cma.2007.02.010
28. Lin, H., Wang, J., Long, A.C., Clifford, M.J., Harrison, P.: Predictive modelling for optimization of textile composite forming. Compos. Sci. Technol. **67**, 3242–3252 (2007). https://doi.org/10.1016/j.compscitech.2007.03.040
29. Chen, S., Harper, L.T., Endruweit, A., Warrior, N.A.: Formability optimisation of fabric preforms by controlling material draw-in through in-plane constraints. Compos. Part A Appl. Sci. Manuf. **76**, 10–19 (2015). https://doi.org/10.1016/j.compositesa.2015.05.006
30. Liang, B., Hamila, N., Peillon, M., Boisse, P.: Analysis of thermoplastic prepreg bending stiffness during manufacturing and of its influence on wrinkling simulations. Compos. Part A Appl. Sci. Manuf. **67**, 111–122 (2014). https://doi.org/10.1016/j.compositesa.2014.08.020
31. Dangora, L.M., Mitchell, C.J., Sherwood, J.A.: Predictive model for the detection of out-of-plane defects formed during textile-composite manufacture. Compos. Part A Appl. Sci. Manuf. **78**, 102–112 (2015). https://doi.org/10.1016/j.compositesa.2015.07.011
32. Döbrich, O., Gereke, T., Diestel, O., Krzywinski, S., Cherif, C.: Decoupling the bending behavior and the membrane properties of finite shell elements for a correct description of the mechanical behavior of textiles with a laminate formulation. J. Ind. Text. **44**, 70–84 (2013). https://doi.org/10.1177/1528083713477442
33. Haanappel, S.P., Ten Thije, R.H.W., Sachs, U., Rietman, B., Akkerman, R.: Formability analyses of uni-directional and textile reinforced thermoplastics. Compos. Part A Appl. Sci. Manuf. **56**, 80–92 (2014). https://doi.org/10.1016/j.compositesa.2013.09.009
34. Dörr, D., Henning, F., Kärger, L.: Nonlinear hyperviscoelastic modelling of intra-ply deformation behaviour in finite element forming simulation of continuously fibre-reinforced thermoplastics. Compos. Part A Appl. Sci. Manuf. **109**, 585–596 (2018). https://doi.org/10.1016/j.compositesa.2018.03.037
35. Launay, J., Hivet, G., Duong, A.V., Boisse, P.: Experimental analysis of the influence of tensions on in plane shear behaviour of woven composite reinforcements. Compos. Sci. Technol. **68**, 506–515 (2008). https://doi.org/10.1016/j.compscitech.2007.06.021
36. Cao, J., Akkerman, R., Boisse, P., Chen, J., Cheng, H.S., de Graaf, E.F., et al.: Characterization of mechanical behavior of woven fabrics: Experimental methods and benchmark results. Compos. Part A Appl. Sci. Manuf. **39**, 1037–1053 (2008). https://doi.org/10.1016/j.compositesa.2008.02.016
37. de Bilbao, E., Soulat, D., Hivet, G., Gasser, A.: Experimental Study of Bending Behaviour of Reinforcements. Exp. Mech. **50**, 333–351 (2010). https://doi.org/10.1007/s11340-009-9234-9
38. Alshahrani, H., Hojjati, M.: A new test method for the characterization of the bending behavior of textile prepregs. Compos. Part A Appl. Sci. Manuf. **97**, 128–140 (2017). https://doi.org/10.1016/j.compositesa.2017.02.027